Pramana – J. Phys. (2021) 95:93
https://doi.org/10.1007/s12043-021-02130-z

Damage evolution in single crystal iron at high strain rate: A molecular dynamics study

SUNIL RAWAT

Indian Institute of Technology Kharagpur, Kharagpur 721 302, India
E-mail: alig.sunil@gmail.com

MS received 14 October 2020; revised 4 December 2020; accepted 19 February 2021

Abstract. We simulate triaxial deformation of a single crystal iron at 10^6 s^{-1} strain rate to investigate the void evolution dynamics in a single crystal iron. We find that the peak tensile pressure is very close to the spall strength of the single crystal iron. As strain rate decreases, the peak tensile pressure approaches the void nucleation threshold of the single crystal iron. The damage of the single crystal iron takes place due to nucleation, growth and coalescence of many voids and not due to the growth of a single void. The void growth rate is very high indicating rapid growth of the voids once nucleated.

Keywords. Void evolution; single crystals; extreme strain rate; molecular dynamics; iron.

PACS Nos 71.15.Pd; 81.40.Lm; 62.20.M; 61.72.Qq; 62.20.mm

1. Introduction

The spall fracture takes place due to nucleation, growth and coalescence of the voids [1]. The spall fracture is a multiscale problem where nucleation, growth and coalescence of voids at the nanoscale leads to the fracture at continuum scale. Therefore, a fundamental understanding of void evolution dynamics at nanoscale is required to understand the fracture at continuum scale.

To understand the void evolution dynamics at nanoscale, molecular dynamics (MD) simulations are commonly used. Many researchers [2–11] performed MD simulations to understand the evolution of voids in metallic systems. Belak [2] in his study on polycrystalline copper found that the yielding of the void at the grain junction occurred at a lower strain than that at the grain centre. Rudd and Belak [3] found that the void nucleation in polycrystalline Cu did not occur at all available junctions. Seppälä *et al* [4] studied the role of stress triaxiality on the growth of pre-existing voids in Cu crystal. Rawat *et al* [6] studied the effect of temperature on the void nucleation and growth parameters for a macroscopic void nucleation and growth (NAG) model [1] for single crystal Cu. Ikkurthi *et al* [8] studied the deformation of Nb and Mo single crystals and reported the void NAG parameters. Rawat and Raole [9] investigated the role of applied strain rate on the void evolution dynamics in single crystal iron. Remington *et al* [10] performed MD simulations to study the spallation in single crystal and nanocrystalline tantalum. Rawat and Chaturvedi [11] investigated the effect of applied loading conditions on the evolution dynamics of voids in single crystal iron.

In our previous work [9], we investigated the role of applied strain rate on the evolution dynamics of voids in a single crystal iron. However, that work was limited to a volumetric strain rate of 1.5×10^8 s^{-1} and did not report the evolution dynamics of voids at 3×10^6 s^{-1} volumetric strain rate. In the current work, we perform triaxial deformation of single crystal iron at 3×10^6 s^{-1} volumetric strain rate to investigate the evolution dynamics of voids in single crystal iron. Note that the applied strain rate (3×10^6 s^{-1}) can be obtained in high velocity impact experiments using gas gun [11,12] and high intensity lasers [14–16]. We use isotropic triaxial loading which is commonly used to understand deformation of materials using MD simulations [2,3,6,7,9,11]. To the best of our knowledge, this is the first report investigating the evolution dynamics of voids in single crystal iron at 3×10^6 s^{-1} volumetric strain rate.

2. Computational method

We simulate isotropic tension in single crystal iron using LAMMPS [17]. The simulation domain contains

Published online: 31 May 2021

2×10^6 atoms corresponding to $100 \times 100 \times 100$ unit cells. The lattice constant is 2.855 Å. The simulation results do not change by further increasing the number of atoms in the simulation domain [11]. We used periodic boundary conditions along three directions. We use the concentration-dependent embedded atom method (CD-EAM) potential [18]. For Fe–Fe interactions, we use parameters obtained by Ackland *et al* [19]. To control the temperature and pressure of the system, we use Nose–Hoover thermostat and barostat, respectively. We use velocity-Verlet algorithm to integrate the equations of motion with a time-step of 1 fs. We equilibrate the system at 300 K and 0 bar pressure upto 20 ps using an isobaric-isothermal ensemble (NPT). Subsequently, we apply isotropic and triaxial tension in the single crystal iron at 10^6 s^{-1} strain rate with 300 K temperature. The volumetric strain rate is 3×10^6 s^{-1}. We use ovito [20] to visualise the simulation results. To compute the void volume fraction, we use post-processor described in [6,21].

3. Results and discussion

In this section, we discuss the pressure–volumetric strain profile, number of voids, overall void volume fraction, average void growth rate and individual void volume fraction.

3.1 *Pressure–volumetric strain profile*

To understand the overall response of the material undergoing deformation, we compute the tensile pressure as a function of volumetric strain. Figure 1 shows the pressure–volumetric strain profile for the single crystal iron. As observed from figure 1, the tensile pressure increases due to the triaxial deformation of the material and at some value of volumetric strain, the turn-around of the pressure takes place. This occurs due to the stress relaxation resulting from the nucleation and growth of the voids. After the turn-around of the pressure, the tensile pressure decreases very rapidly due to the exponential void growth. Note that the peak tensile pressure is 17.95 GPa which is very close to the spall strength (17.8–20.3 GPa) of the single crystal iron at 3–4 $\times$ 10^8 strain rate [22]. The spall strength of single crystal iron at 5×10^6 s^{-1} strain rate is 7.6 GPa [23]. The difference in the values of spall strength of single crystal iron could be due to the presence of impurity, different kinds of defects and applied strain rate in the sample. Note that the spall strength of a perfect single crystal iron would always be higher than the real crystals due to the presence of defects. The peak tensile pressure for the single crystal iron at different volumetric strain-rates [9] is shown in table 1. As observed from table 1 the peak tensile pressure decreases with a decrease in the applied volumetric strain rate. Rudd [24] performed MD simulations at (10^6–10^9) s^{-1} strain rates to predict the growth threshold for a pre-existing void in BCC metals and found that the peak tensile pressure became the growth threshold as the applied strain rate was decreased to 10^6 s^{-1} strain rate. Therefore, for lower strain rates, the peak tensile pressure should become the threshold for void nucleation. However, due to computational limitations, it is difficult to perform simulations at strain rates $< 10^6$.

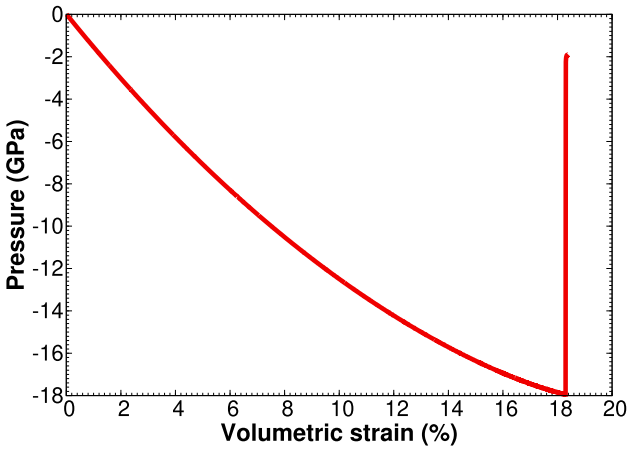

Figure 1. Tensile pressure as a function of volumetric strain for the single crystal iron.

Table 1. Peak tensile pressure at different volumetric strain rates [9].

Volumetric strain rate (s^{-1})	Peak tensile pressure (GPa)
1.5×10^{10}	18.35
9×10^9	18.25
3×10^9	18.14
1.5×10^9	18.09
3×10^8	18.03
1.5×10^8	18.02
3×10^7	17.98
3×10^6	17.95

3.2 *Number of voids*

To understand whether the evolution of damage takes place due to the nucleation and growth of a single void or many voids, we compute the number of voids as a function of volumetric strain. Note that the number of voids can be measured in the experiments [25]. However, the *in-situ* measurement of temporal evolution of the number of voids in high strain rate experiments is quite difficult. To compute the number of voids, we divide the whole simulation domain into cubic voxels.

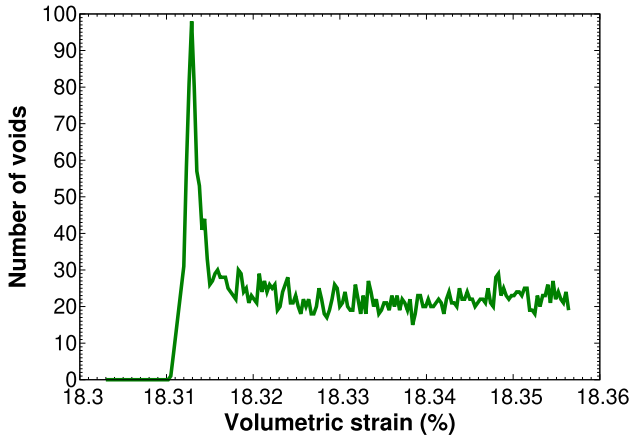

Figure 2. Number of voids as a function of volumetric strain.

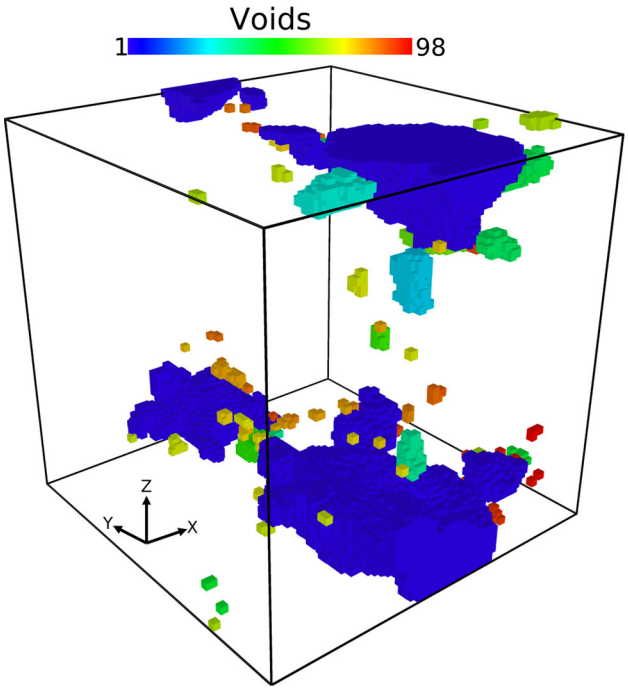

Figure 3. Spatial distribution of peak number of voids (figure 2) in the single crystal iron. The MD data are post-processed to get the distribution of voids. Different colours are assigned to different voids to distinguish them from each other.

Initially, all cubic voxels will be filled and there will be no void. When voids are created, some of the voxels become empty. These empty voxels are then counted to estimate the number of voids at any instant of time. Figure 2 shows the number of voids as a function of volumetric strain. As observed from figure 2, the number of voids increases up to some time point, reaches a peak and then decreases. The number of voids increases due to the nucleation of new voids. The nucleation and coalescence processes of the voids compete with each other and the dominance of the coalescence process over the nucleation process leads to a peak in the number of voids–volumetric strain profile. The number of voids decreases due to the dominance of the coalescence process over the nucleation process. The fluctuations in the number of voids is due to the competition between the nucleation and coalescence processes. Note that the damage evolution takes place due to the nucleation, growth and coalescence of the many voids and not due to the nucleation and growth of a single void.

The spatial distribution of the peak number of voids (figure 2) is shown in figure 3. The MD data are post-processed to show the distribution of voids in the single crystal iron. As observed from figure 3, one void cluster is dominant over the others. A single cubic voxel indicates an independent void while a group of cubic voxels refers to the void cluster [11].

3.3 *Void volume fraction*

To understand the void spaces in the material, we compute the void volume fraction which is defined as the ratio of volume of the voids to the total volume of the simulation domain. It shows the collective behaviour of all the nucleated, growing and coalesced voids and is computed as the ratio of the total number of empty voxels to the total number of cubic voxels. It is an experimentally measurable quantity [1,26]. Figure 4 shows the void volume fraction as a function of volumetric strain for the single crystal iron. As observed from figure 4, the void volume fraction increases exponentially due to the exponential growth of the voids and then saturates. Note that at high volumetric strain rates (e.g. 1.5×10^{10} s^{-1}), the void volume fraction does not saturate and grows linearly with volumetric strain [9]. The void volume fraction–volumetric strain profile can be divided into three regimes: (a) nucleation process dominating regime – in this regime the void volume due to nucleation dominates over the growth. This corresponds to the initial portion of the void volume fraction–volumetric strain graph, (b) growth process dominating regime – in this regime the void volume due to growth dominates over the nucleation. This corresponds to the exponential portion of the void volume fraction–volumetric strain graph and (c) coalescence process dominating regime – in this regime the void volume due to coalescence dominates over the growth. This corresponds to saturation followed by sluggish portion of the void volume fraction–volumetric strain graph. Note that the void volume fraction is due to nucleation, growth and coalescence of many voids and not due to the growth of a single void.

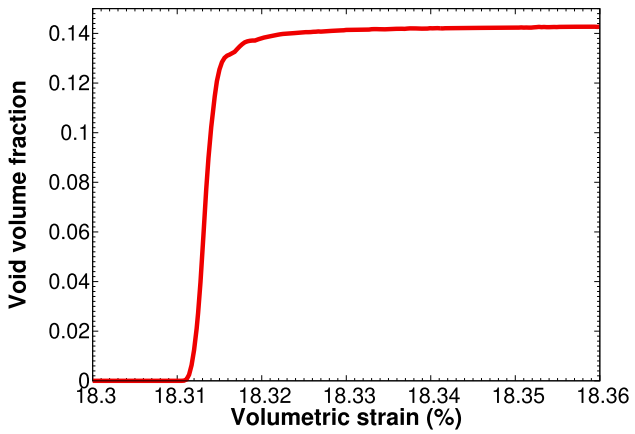

Figure 4. Void volume fraction as a function of volumetric strain for the single crystal iron.

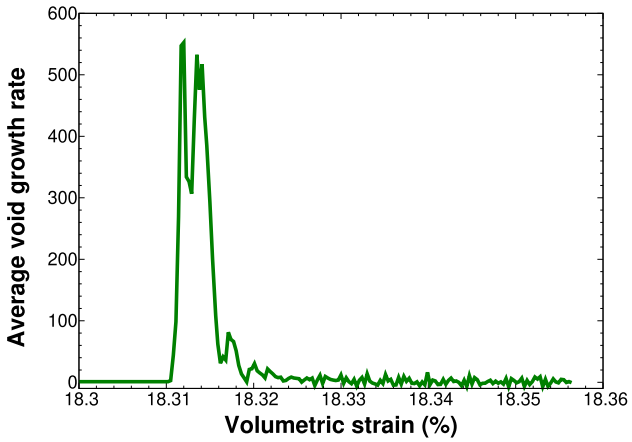

Figure 5. Average void growth rate as a function of volumetric strain for single crystal iron.

3.4 *Average void growth*

To understand the growth rate of the voids at 3×10^6 s^{-1} volumetric strain rate, we compute the average void growth rate as a function of volumetric strain. If $\Phi_j(\varepsilon_v)$ is the volume fraction of the jth void at ε_v strain and $\Phi_j(\varepsilon_v - \Delta\varepsilon_v)$ is the volume fraction of the jth void at $(\varepsilon_v - \Delta\varepsilon_v)$ strain, then the average void growth rate at ε_v strain is given as $\sum_{j=1}^{N^g} \Delta\Phi_j(\varepsilon_v)/N^g(\varepsilon_v)\Delta\varepsilon_v$, where N^g is the number of growing voids, $\Delta\varepsilon_v$ is the change in volumetric strain and $\Delta\Phi_j(\varepsilon_v)$ is the change in volume fraction of the jth void. Note that in this calculation, we have excluded the number of new voids. Figure 5 shows the average void growth rate as a function of volumetric strain for the single crystal iron. It is observed from figure 5 that the average growth rate of the voids is very high indicating the rapid growth of voids once nucleated. In this regard, it should be noted that Meyers and Aimone [27] in their study on the nucleation and growth of voids found that no void was smaller than 1 μm. They suggested that either voids of 1 μm size nucleate in the material or their rapid growth leads to the void size of 1 μm. On the basis of results in figure 5, we can say that the micron size voids are possibly due to the rapid growth of the voids.

3.5 *Individual void volume fraction*

In high strain rate experiments, it is very difficult to track the evolution of an individual void. Note that the volume fraction of the individual voids can be measured in the experiments [1,25]. To understand the evolution of a void, we compute the individual void volume fraction as a function of volumetric strain. As it is difficult to show the evolution of all the nucleated voids, we consider only the most dominant voids at the end of the simulation. Figure 6 shows the individual void volume fraction as a function of volumetric strain. As observed from figure 6, all the voids do not contribute equally to the overall void volume fraction. Void 1 contributes most to the overall void volume fraction while voids 2 and 3 contribute very less to the overall void volume fraction. Note that the jump in individual void volume fraction (e.g. void 1) indicates void coalescence. Note also that the rupture of the single crystal iron takes place due to the nucleation, growth and coalescence of many voids (see figure 3) and not due to the growth of a single void. At some time points, there are several voids (see figure 3) which have significant contribution to the overall void volume fraction. These voids coalesce to void 1. This means that at the end of the simulation, void 1 contributes the most to the overall void volume fraction.

4. Summary and conclusions

We simulate triaxial deformation of the single crystal iron at 3×10^6 s^{-1} volumetric strain rate to investigate the evolution dynamics of voids in the single crystal iron. We compute tensile pressure, number of voids, void volume fraction, average void growth rate and individual void volume fraction to understand the deformation of the single crystal iron. The peak tensile pressure is very close to the spall strength of the single crystal iron reported in the experiments. As strain rate decreases, the peak tensile pressure approaches the void nucleation threshold of the single crystal iron. The damage of the single crystal iron takes place due to nucleation, growth and coalescence of many voids and not due to the growth of a single void. Individual void volume fraction evolves with discrete jumps due to coalescence of the voids. All voids do not make significant contribution to the total

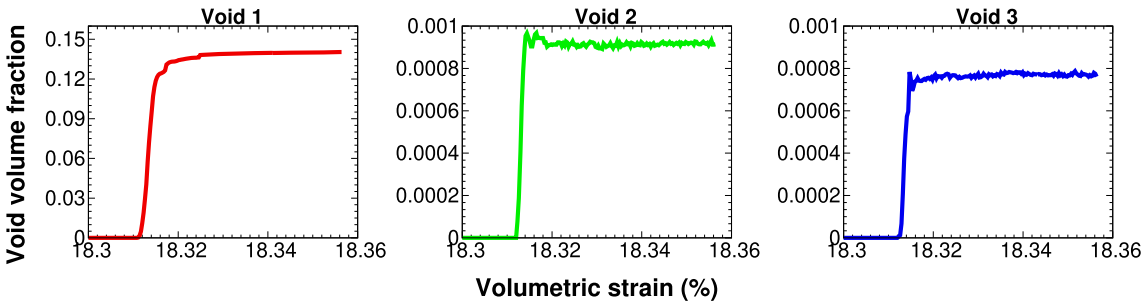

Figure 6. Individual void volume fraction as a function of volumetric strain for the single crystal iron.

void volume fraction. The void growth rate is very high indicating the rapid growth of the voids once nucleated.

References

[1] D R Curran, L Seaman and D A Shockey, *Phys. Rep.* **147**, 253 (1987)

[2] J Belak, *J. Computer-aided Mater. Design* **5**, 193 (1998)

[3] Robert E Rudd and James F Belak, *Comput. Mater. Sci.* **24**, 148 (2002)

[4] E T Seppälä, J Belak and R E Rudd, *Phys. Rev. B* **69**, 134101 (2004)

[5] E T Seppälä, J Belak and R E Rudd, *Phys. Rev. Lett.* **93**, 245503 (2004)

[6] S Rawat, M Warrier, S Chaturvedi and V M Chavan, *Model. Simul. Mater. Sci. Eng.* **19**, 025007 (2011)

[7] S Rawat, M Warrier, S Chaturvedi and V R Ikkurthi, *Pramana – J. Phys.* **83**, 265 (2014)

[8] V R Ikkurthi, H Hemani, R Sugandhi, S Rawat, P Pahari, M Warrier and S Chaturvedi, *Proc. Eng.* **173**, 1177 (2017)

[9] Sunil Rawat and P M Raole, *Comput. Mater. Sci.* **154**, 393 (2018)

[10] T P Remington, E N Hahn, S Zhao, R Flanagan, J C E Mertens, S Sabbaghianrad, Terence G Langdon, C E Wehrenberg, B R Maddox, D C Swift *et al*, *Acta Mater.* **158**, 313 (2018)

[11] Sunil Rawat and Shashank Chaturvedi, *Phil. Mag.* pp. 1–23 (2020)

[12] Roger W Minich, James U Cazamias, Mukui Kumar and Adam J Schwartz, *Metall. Mater. Trans. A* **35**, 2663 (2004)

[13] D C Erlich, D A Shockey and L Seaman, in: *Shock waves in condensed matter-1981* (AIP Publishing, 1982) Vol. 78, pp. 402–406

[14] H Jarmakani, B Maddox, C T Wei, D Kalantar and M A Meyers, *Acta Mater.* **58**, 4604 (2010)

[15] G I Kanel, S V Razorenov, A V Utkin, V E Fortov, K Baumung, H U Karow, D Rusch and V Licht, *J. Appl. Phys.* **74**, 7162 (1993)

[16] Shalom Eliezer, Irith Gilath and Tuvia Bar-Noy, *J. Appl. Phys.* **67**, 715 (1990)

[17] Steve Plimpton, *J. Comput. Phys.* **117**, 1 (1995)

[18] A Caro, J Hetherly, A Stukowski, M Caro, E Martinez, S Srivilliputhur, L Zepeda-Ruiz and Michael Nastasi, *J. Nucl. Mater.* **418**, 261 (2011)

[19] G J Ackland, M I Mendelev, D J Srolovitz, S Han and A V Barashev, *J. Phys.: Condens. Matter* **16**, S2629 (2004)

[20] Alexander Stukowski, *Model. Simul. Mater. Sci. Eng.* **18**, 015012 (2009)

[21] H Hemani, M Warrier, N Sakthivel and S Chaturvedi, *J. Mol. Graphics Model.* **50**, 134 (2014)

[22] Sergei Igorevich Ashitkov, Pavel Sergeevich Komarov, Mikhail Borisovich Agranat, Gennadii Isaakovich Kanel and Vladimir Evgen'evich Fortov, *JETP Lett.* **98**, 384 (2013)

[23] Sergei Vladimirovich Razorenov, Gennadii Isaakovich Kanel and Vladimir Evgen'evich Fortov, *J. Exp. Theor. Phys. Lett.* **80**, 348 (2004)

[24] Robert E Rudd, *Phil. Mag.* **89**, 3133 (2009)

[25] Lynn Seaman, Donald R Curran and Donald A Shockey, *J. Appl. Phy.* **47**, 4814 (1976)

[26] P G Kossakowski, *Arch. Metall. Mater.* **62**, 167 (2017)

[27] Marc André Meyers and Catherine Taylor Aimone, *Prog. Mater. Sci.* **28**, 1 (1983)